

# AV-CrossNet: an Audiovisual Complex Spectral Mapping Network for Speech Separation By Leveraging Narrow- and Cross-Band Modeling

Vahid Ahmadi Kalkhorani, Cheng Yu, Anurag Kumar, Ke Tan, Buye Xu, DeLiang Wang, *Fellow, IEEE*

**Abstract**—Adding visual cues to audio-based speech separation can improve separation performance. This paper introduces AV-CrossNet, an audiovisual (AV) system for speech enhancement, target speaker extraction, and multi-talker speaker separation. AV-CrossNet is extended from the CrossNet architecture, which is a recently proposed network that performs complex spectral mapping for speech separation by leveraging global attention and positional encoding. To effectively utilize visual cues, the proposed system incorporates pre-extracted visual embeddings and employs a visual encoder comprising temporal convolutional layers. Audio and visual features are fused in an early fusion layer before feeding to AV-CrossNet blocks. We evaluate AV-CrossNet on multiple datasets, including LRS, VoxCeleb, and COG-MHEAR challenge. Evaluation results demonstrate that AV-CrossNet advances the state-of-the-art performance in all audiovisual tasks, even on untrained and mismatched datasets.

**Index Terms**—Audiovisual speech enhancement, audiovisual target speaker extraction, audiovisual speaker separation, CrossNet, AV-CrossNet.

## I. INTRODUCTION

IN real-world scenarios, speech signals are often corrupted by acoustic interference, such as background noise, room reverberation, and competing speakers. Such interference significantly degrades speech understanding in both human and computer communications. To mitigate these challenges, speech separation techniques have been developed to separate the target speech signal from interfering sources. In the past decade, many algorithms have been developed for audio-based speech separation [1]. Traditional approaches include speech enhancement that analyzes spectral and statistical properties of speech and noise in order to remove or attenuate background noise [2], and computational auditory scene analysis (CASA) that exploits auditory cues like pitch, onset/offset, and spatial location to segregate sound sources [3]. Since the formulation of speech separation as supervised learning, deep neural networks (DNNs) have become the mainstream approach [1].

Talker-independent speaker separation faces a so-called permutation ambiguity problem [4], referring to the challenge of consistently assigning speakers with DNN output layers during

training. This problem can be resolved by deep clustering [5] or permutation invariant training [5]. Recent years have seen major progress in speaker separation. Notable methods include Conv-TasNet [6], deep CASA [7], DPRNN [8], and TF-GridNet [9]. Despite their impressive results, current speaker separation algorithms have difficulty dealing with audio recordings with partly overlapped speech and same-talker utterances scattered in time [10]–[12]. Target speaker extraction presents an alternative way to address the speaker separation problem. This approach attempts to separate the speech of the target or desired speaker by leveraging discriminative cues that differentiate the target talker from other speakers. Different discriminative cues have been explored such as speaker embedding or identity [13], onset time [14], and visual cues [15].

While existing speaker separation and target speaker extraction methods rely mainly on audio signals, human perception makes use of both auditory and visual cues for speech understanding in multi-talker and adverse acoustic environments [16], [17]. Inspired by this multi-modal perception, audiovisual (AV) speech separation aims to incorporate visual information from facial attributes and movements to improve the separation of speech sources [15].

The audio and video modalities exhibit distinct attributes that complement each other for perception. For instance, audio signals are degraded by acoustic interference, which does not impact vision. Visual inputs are affected by poor lighting, limited visual view, and object occlusion, which do not impede audition. By fusing auditory and visual modalities, audiovisual models can achieve more robust separation than audio-only methods, especially in highly noisy environments where auditory cues become unreliable. Additionally, the presence of visual cues may help resolve permutation ambiguity in talker-independent speaker separation.

In recent years, the availability of large-scale audiovisual datasets like LRS2 [18], VoxCeleb2 [19], and AVSpeech [20] has led to the development of promising techniques for audiovisual speaker separation (AVSS) [20], [21], audiovisual speech recognition (AVSR) [22], [23], audiovisual speech enhancement (AVSE) [24], [25], and audiovisual target speaker extraction (AVTSE) [26]. Given auditory and visual cues, the task of AVSS is to separate the speech signals of multiple speakers and AVSE aims to separate a single speech signal from non-speech background noise. The goal of AVTSE is to extract the speech signal of a target speaker from a mixture of multiple speakers.

Vahid Ahmadi Kalkhorani and Cheng Yu are with the Department of Computer Science and Engineering, Ohio State University, Columbus, OH 43210 USA (e-mail: ahmadikalkhorani.1@osu.edu; yu.3500@osu.edu). Anurag Kumar, Ke Tan, and Buye Xu are with Meta Reality Labs, Redmond, WA 20004 USA (e-mail: anuragkr90@meta.com; tanke1116@meta.com; xub@meta.com). DeLiang Wang is with the Department of Computer Science and Engineering and the Center for Cognitive and Brain Sciences, Ohio State University, Columbus, OH 43210 USA (e-mail: dwang@cse.ohio-state.edu).

Early studies in audiovisual speaker separation primarily rely on magnitude-domain time-frequency (T-F) masking [27]–[32]. More recently, time-domain models have been proposed [33]–[36], and these models employ learnable encoder-decoder modules with demonstrated success in AVSS and AVTSE. Time-domain models usually have more parameters compared to T-F domain approaches and operate on very short windows of signals for end-to-end speaker separation/extraction.

The introduction of TF-GridNet [9], a complex spectral mapping network for speech separation in single- and multi-channel settings, has renewed interest in T-F domain models. This approach uses larger window lengths and shifts compared to time-domain models, and produces high speech separation performance. The audiovisual counterpart of TF-GridNet, AVTF-Gridnet [37], also shows strong results in AVSS by employing cross-attention audiovisual fusion. SAV-GridNet [38], another audiovisual TF-GridNet model, achieves the best performance in the second COG-MHEAR AVSE challenge in 2023 and substantially outperforms other entries [39]. SAV-GridNet has two scenario-specific models: AV-GridNet<sub>n</sub> for AVSE and AV-GridNet<sub>s</sub> for AVTSE, and a scenario classifier to guide the system to the model trained for the matched scenario. Despite impressive results, the two expert models trained in their respective scenarios complicate the inference process of AV-GridNet. From the methodological perspective, the use of a scenario classifier commits the system to a particular task early on, and classification errors cannot be corrected by later processing. Moreover, a unified model for AVSE and AVTSE can also enhance learning by leveraging the relationship between the two tasks.

Another recently developed complex spectral mapping model, CrossNet [40], yields comparable performance to TF-GridNet, but with reduced computational expenses. CrossNet is an audio-based speech separation model that can be applied to speech enhancement and speaker separation in monaural and multi-channel recordings [40]. CrossNet has a compact architecture and is easier to train compared to TF-GridNet which utilizes recurrent layers.

In this paper, we propose AV-CrossNet, an audiovisual system based on the CrossNet architecture, for AVSE, AVSS, and AVTSE tasks. We employ a widely adopted visual front-end, DeepAVSR [18], to extract visual embeddings from video frames. AV-CrossNet includes an early audiovisual fusion layer and positional encoding that preserves the temporal order of audiovisual fused features. In addition to proposing AV-CrossNet, we demonstrate that it achieves the top performance on multiple trained and untrained AV datasets. Compared to recently proposed complex spectral mapping models, AV-CrossNet can be trained more efficiently as it has no recurrent layers and employs half-precision training. Another contribution of this paper is that we handle the permutation ambiguity problem in speaker separation by leveraging visual cues.

The rest of this paper is organized as follows. In Section II, we formulate audiovisual speaker separation and target speaker extraction problems. In Section III, we describe AV-CrossNet in detail. Experimental setup is provided in Section IV. In Section V, we present experimental and comparison results.

Section VI concludes this paper.

We provide the AV-CrossNet code at <https://github.com/ahmadikalkhorani/AVCrossNet>.

## II. PROBLEM FORMULATION

For a mixture of  $C$  speakers in a noisy environment captured by a single microphone, the recorded mixture in the time domain  $y(t)$  can be modeled in terms of the clean signals  $s_c(t)$  and background noises  $n(t)$ , as

$$y(t) = \sum_{c=1}^C s_c(t) + n(t), \quad (1)$$

where  $t$  denotes discrete time. In the short-time Fourier transform (STFT) domain, the model is expressed as:

$$Y(m, f) = \sum_{c=1}^C S_c(m, f) + N(m, f), \quad (2)$$

where  $m$  indexes time frames and  $f$  frequency bins.  $\mathbf{Y}$ ,  $\mathbf{S}_c$ , and  $\mathbf{N} \in \mathbb{C}^{M \times F}$  represent the complex spectrograms of the mixture, the clean signal of speaker  $c$ , and background noise, respectively, and  $M$  and  $F$  denote the number of time frames and frequency bins, respectively. Audiovisual speaker separation based on complex spectral mapping trains a DNN to estimate the real and imaginary parts of the signal of each speaker given the mixture  $\mathbf{Y}$  and visual stream of each speaker  $\mathbf{V}_c \in \mathbb{R}^{M_v \times 3 \times h \times w}$ . This is defined as

$$\hat{\mathbf{S}}_1, \dots, \hat{\mathbf{S}}_C = \text{DNN}_\theta(\mathbf{Y}, \mathbf{V}_1, \dots, \mathbf{V}_C), \quad (3)$$

where  $\text{DNN}_\theta$  denotes DNN parameterized by  $\theta$ .

In the case of AVTSE and AVSE,  $C = 1$ , and the goal is to estimate the complex spectrogram of the target speaker (or speech signal)  $\mathbf{S}_T$  from the mixture  $\mathbf{Y}$  and the visual stream of the target speaker  $\mathbf{V}_T \in \mathbb{R}^{M_v \times 3 \times h \times w}$ .

## III. SYSTEM DESCRIPTION

Fig. 1 shows the diagram of the proposed system. AV-CrossNet comprises an audio encoder layer, a visual encoder,  $B$  separator blocks referred to as AV-CrossNet blocks, and a decoder layer. Before processing, we normalize the input signal by its variance to ensure comparable energy levels for all signals processed by AV-CrossNet. We restore the predicted signal's scale using the same variance. We apply STFT to the normalized signal, stack the real and imaginary (RI) parts, and send them to the audio encoder layer. This layer learns to extract acoustic features from the input in the STFT domain. The visual encoder extracts visual features from a whole-face image of a speaker and upsamples the result to match the time resolution of the audio stream. Audio and visual features are then fused in the AV-fusion block and passed to AV-CrossNet blocks. These blocks are responsible for separating speakers or extracting the target speaker given the fused multi-modal features. Each AV-CrossNet block comprises a narrow-band module, a cross-band module, and a global multi-head self-attention (GMHSA) module. The GMHSA module captures global correlations, while the cross-band module captures

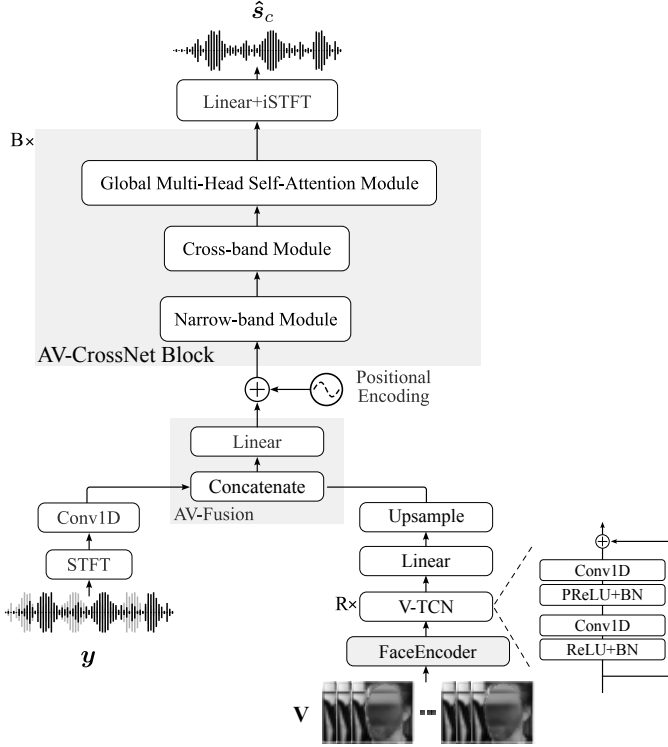


Fig. 1: Diagram of the proposed AV-CrossNet system for AVSE and AVTSE. For AVSS, a video component is added for each speaker. Faces in this figure are blurred for privacy reasons.

cross-band correlations. The narrow-band module captures correlations at neighboring frequency bins. Finally, the decoder layer maps the separated features to a T-F representation, which is then converted back to the time domain using inverse short-time Fourier transform (iSTFT).

#### A. Audio Encoder

We stack RI parts of the input signal in the STFT domain  $\hat{\mathbf{Y}} \in \mathbb{R}^{M \times 2 \times F}$  and feed them to the audio encoder. As shown in Fig. 1, the audio encoder comprises a convolutional layer with the kernel, stride, and output channel dimension of  $k_a$ , 1, and  $H$ , respectively. The audio encoder extends the feature dimension from 2 (RI) to  $H$ . This can be derived as

$$\hat{\mathbf{Y}} = [\mathbf{Y}^{(r)}, \mathbf{Y}^{(i)}], \quad \hat{\mathbf{Y}} \in \mathbb{R}^{M \times 2 \times F}, \quad (4a)$$

$$\tilde{\mathbf{Y}} = \text{Conv1D}(\hat{\mathbf{Y}}), \quad \tilde{\mathbf{Y}} \in \mathbb{R}^{M \times H \times F}, \quad (4b)$$

where superscripts  $(r)$  and  $(i)$  indicate real and imaginary parts, respectively, and  $[(\cdot), (\cdot)]$  denotes the stacking operation.

#### B. Visual Encoder

The visual encoder consists of a face encoder, a visual temporal convolutional network (V-TCN) module, a linear layer, and an up-sampling layer. We assume that all videos are recorded at 25 frames per second and that each talker's face is cropped and scaled to an image with a shape of

$1 \times 112 \times 112$ . The face encoder takes the whole face gray-scaled image  $\mathbf{V} \in \mathbb{R}^{M_v \times 1 \times 112 \times 112}$  and converts each frame to an embedding vector yielding  $\mathbf{V}' \in \mathbb{R}^{M_v \times F_v}$ , where  $M_v$  represents the number of video frames and  $F_v$  indicates the embedding dimension. V-TCN [6], [41] comprises two activation functions and batch normalization (BN) layers, with each followed by a 1D convolutional layer (Conv1D). The activation functions are rectified linear unit (ReLU) and parametric rectified linear unit (PReLU). The input and output channels of both Conv1Ds are equal to the face encoder's output dimension  $F_v$ . The kernel size of the first and second Conv1D is 1 and 3, respectively. The V-TCN module is repeated for  $R = 5$  times with residual connections within each module. A linear layer is employed after the V-TCN blocks, and it converts the feature dimension from  $F_v$  to  $F$ . Finally, the upsampling layer interpolates the feature matrix in the time dimension to match the time resolution  $T$  of auditory features. These steps are formulated as follows

$$\mathbf{V}'_c = \text{FaceEncoder}(V), \quad \mathbf{V}'_c \in \mathbb{R}^{M_v \times 1 \times F_v}, \quad (5a)$$

$$\mathbf{V}''_c = \text{V-TCN}(V'_c), \quad \mathbf{V}''_c \in \mathbb{R}^{M_v \times 1 \times F}, \quad (5b)$$

$$\mathbf{V}'''_c = \text{Linear}(V''_c), \quad \mathbf{V}'''_c \in \mathbb{R}^{M_v \times H \times F}, \quad (5c)$$

$$\tilde{\mathbf{V}}_c = \text{Upsample}(V'''_c), \quad \tilde{\mathbf{V}}_c \in \mathbb{R}^{M \times H \times F}. \quad (5d)$$

In the case of AVSS,  $C > 1$ , and we concatenate the visual features of all speakers along the channel dimension. This is defined as

$$\tilde{\mathbf{V}} = [\tilde{\mathbf{V}}_1, \tilde{\mathbf{V}}_2, \dots, \tilde{\mathbf{V}}_C], \quad \tilde{\mathbf{V}} \in \mathbb{R}^{M \times (C \times H) \times F}. \quad (6)$$

#### C. Audiovisual Fusion

The audiovisual fusion module, denoted as AV-Fusion in Fig. 1, receives auditory  $\tilde{\mathbf{Y}} \in \mathbb{R}^{M \times H \times F}$  and visual features  $\tilde{\mathbf{V}} \in \mathbb{R}^{M \times (C \times H) \times F}$  as input and concatenates them along the second dimension. Then, we use a linear layer to convert the dimension back to  $H$ . This is defined as

$$\mathbf{X} = [\tilde{\mathbf{Y}}, \tilde{\mathbf{V}}], \quad \mathbf{X} \in \mathbb{R}^{M \times (C \times H + H) \times F}, \quad (7a)$$

$$\mathbf{X}' = \text{Linear}(\mathbf{X}), \quad \mathbf{X}' \in \mathbb{R}^{M \times H \times F}. \quad (7b)$$

#### D. Positional Encoding

To preserve relative positions of the audiovisual features in time, we employ random-chunk positional encoding (RCPE) [40], which selects a contiguous chunk of positional embedding vectors from a pre-computed positional encoding (PE) matrix. For RCPE, we start by defining PE as a combination of sine and cosine functions [42] as

$$\text{PE}(m, 2i) = \sin\left(\frac{m}{10000^{2i/(F \times H)}}\right), \quad (8a)$$

$$\text{PE}(m, 2i + 1) = \cos\left(\frac{m}{10000^{2i/(F \times H)}}\right). \quad (8b)$$

where  $i$  indexes the embedding dimension. Let the fused audiovisual feature matrix have  $L$  time frames, where  $L = M$  for training and validation, and  $L \in [1, L^{\max}]$  for testing, with

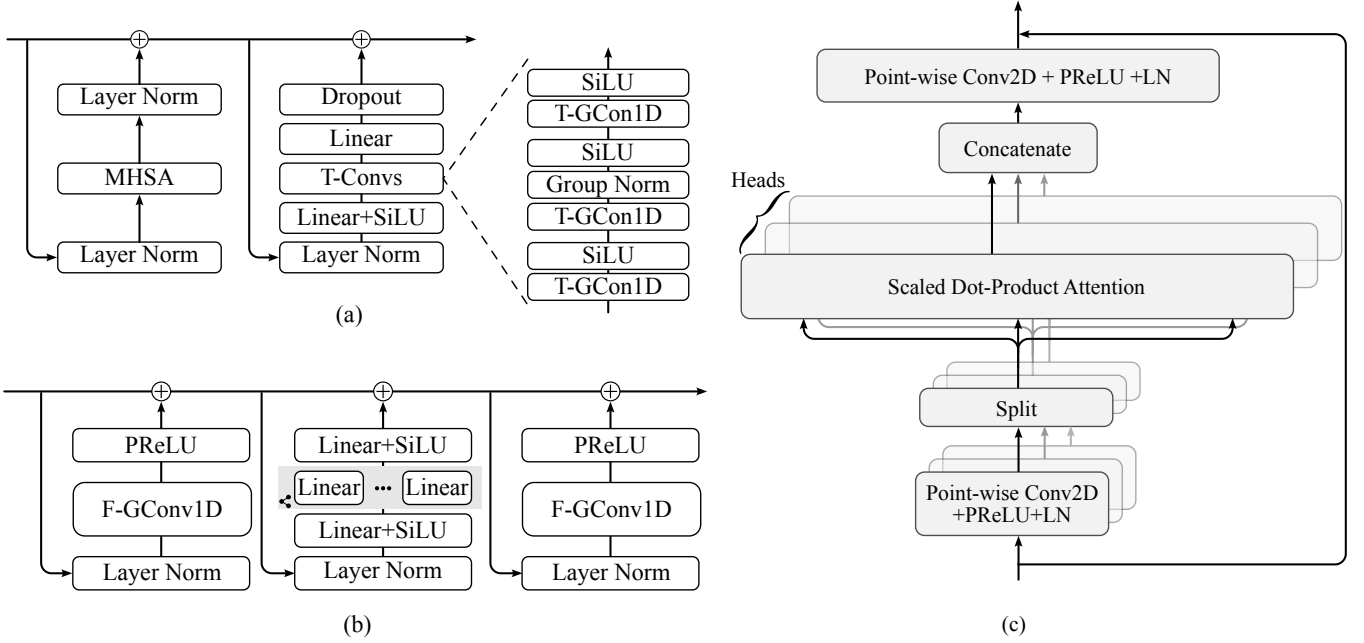


Fig. 2: AV-CrossNet building blocks. (a) Narrow-band module. (b) Cross-band module. (c) Global multi-head self-attention module.

$L^{\max} > M$  denoting the maximum desired sequence length in the test set. We define RCPE as follows. When the model is in the training mode, we select a random PE chunk from frame  $\tau$  to  $\tau + L - 1$ , where  $\tau$  is drawn randomly from  $[1, L^{\max} - L + 1]$ . When the model is in the test or validation mode, we select the first  $L$  embedding vectors, i.e.,  $\tau = 1$ . We obtain positional encoding vectors as shown below

$$\text{RCPE}(L) = \begin{cases} \text{PE}[\tau : \tau + L - 1, \dots], & \text{if training} \\ \text{PE}[1 : L, \dots], & \text{else} \end{cases} \quad (9)$$

It has been shown that RCPE generalizes better for out-of-distribution sequence lengths [40]. Additionally, RCPE has no learnable parameter and has a negligible computational cost. Finally, we reshape and add the selected PEs to input features:

$$\mathbf{X}'' = \mathbf{X}' + \text{Reshape}(\text{RCPE}(L)). \quad (10)$$

### E. AV-CrossNet Block

1) *Narrow-band Module*: The narrow-band module, as illustrated in Fig. 2(a), comprises two components: multi-head self-attention (MHSA) and time-convolutional (T-Conv). The MHSA component is encompassed by two layer normalization (LN) layers and operates on the input feature matrix  $\mathbf{X}''$ . The output of the MHSA component is subsequently added to the input of the narrow-band module. Notably, this module can function as an additional audiovisual fusion layer, similar to an attentive audiovisual fusion mechanism [35], [37]. The T-Conv component consists of the following layers: an LN layer, a linear layer with a subsequent sigmoid-weighted linear unit (SiLU) activation, a T-Conv layer, and a final linear layer. The initial linear layer within this component increases the feature

dimension in the input from  $H$  to  $H''$ , while the last linear layer reverts the feature dimension back to  $H$ . Finally, we obtain the output of the narrow-band module by passing the result to a Dropout layer and adding the module's input.

2) *Cross-band Module*: To model cross-band correlations in the input signal, we utilize the cross-band module introduced in [40], [43]. This module, depicted in Fig. 2(b), incorporates two frequency-convolutional components and a full-band linear component. The frequency-convolutional components are designed to capture correlations among neighboring frequencies. Each comprises an LN layer, a grouped convolution layer along the frequency axis (F-GConv1d), and a PReLU activation function. In the full-band linear component, we initially employ a linear layer followed by a SiLU activation function to reduce the number of hidden channels from  $H$  to  $H'$ . Subsequently, a series of linear layers along the frequency axis is applied to capture full-band features. Each feature channel is associated with a dedicated linear layer denoted as  $\text{Linear}_i$  for  $i = 1, \dots, H'$ , as illustrated in Fig. 2(b). Notably, the parameters of these linear layers are shared among all AV-CrossNet blocks, similar to [40]. Finally, the output of the component is obtained by increasing the number of channels back to  $H$  using a linear layer with SiLU activation and adding it to the original input of this module.

3) *Global Multi-Head Self-Attention Module*: Figure 2(c) illustrates the GMHSA module. A convolutional layer with  $L(2E + H/L)$  output channels extracts frame-level features from each T-F unit. The output is then divided into  $L$  queries  $Q^l \in \mathbb{R}^{E \times F \times T}$ , keys  $K^l \in \mathbb{R}^{E \times F \times T}$ , and values  $V^l \in \mathbb{R}^{H/L \times F \times T}$ , where  $E$  represents the output channel dimension of the point-wise convolution, and  $l$  indexes the head number. We apply MHSA to these embeddings to capture global dependencies. The outputs from all heads are concatenated and

processed by another point-wise convolution with an output dimension of  $H$ , followed by a PReLU activation and an LN layer. The resulting values are added to the input of the GMHSA to produce the final output.

#### F. Decoder

As shown in Fig. 1, the decoder uses a linear layer to convert the feature dimension from  $H$  to  $2 \times C$  resulting in  $Z \in \mathbb{R}^{C \times 2 \times M \times F}$ , which is then converted to  $C$  waveform signals using iSTFT.

#### G. Loss Function

We employ a combination of magnitude loss,  $\mathcal{L}_{\text{Mag}}$ , and scale-invariant signal-to-distortion ratio (SI-SDR) loss,  $\mathcal{L}_{\text{SI-SDR}}$ , similar to [9], [44]. We use the standard form of SI-SDR where the target signal is scaled to match the scale of the estimated signal. Also, we scale the magnitude loss by the  $L_1$  norm of the magnitude of the target signal in the STFT domain similar to [44]. These loss functions are defined as

$$\mathcal{L} = \mathcal{L}_{\text{Mag}} + \mathcal{L}_{\text{SI-SDR}}, \quad (11a)$$

$$\mathcal{L}_{\text{Mag}} = \frac{\| |\text{STFT}(\hat{s}_c)| - |\text{STFT}(s_c)| \|_1}{\| |\text{STFT}(s_c)| \|_1}, \quad (11b)$$

$$\mathcal{L}_{\text{SI-SDR}} = - \sum_{c=1}^C 10 \log_{10} \frac{\|s_c\|_2^2}{\|\hat{s}_c - \alpha_c s_c\|_2^2}, \quad (11c)$$

$$\alpha_c = \frac{s_c^T \hat{s}_c}{s_c^T s_c}. \quad (11d)$$

In the above equations,  $L_1$  norm is denoted by  $\|\cdot\|_1$ ,  $|\cdot|$  represents the magnitude operator,  $\alpha_c$  is the scaling factor, and  $(\cdot)^T$  denotes the transpose operation. To resolve permutation ambiguity during the AVSS training, we order the target signals in the same order as the visual streams. Thus the model learns to map each talker’s signal to the corresponding output layer consistently.

### IV. EXPERIMENTAL SETUP

#### A. Data Preparation

We evaluate AV-CrossNet on four tasks, i.e. audiovisual target speaker extraction, audiovisual speaker separation, audiovisual speaker separation in noisy environments, and audiovisual speech enhancement.

1) *Audiovisual Speaker Separation in Clean Environments:* We use LRS2 [18], LRS3 [45], VoxCeleb2 [19] datasets for evaluating AVSS. LRS2 contains thousands of single-talker BBC video clips. We derive the LRS2-2Mix dataset from LRS2 by mixing different speakers with target-to-interferer ratio (TIR) ranging from -5 to +5 dB. The training set comprises 11 hours of mixed audio, while the validation set has 3 hours. The test set is the same one used in prior studies [46]. LRS3 consists of thousands of spoken sentences from TED and TEDx videos. To create the LRS3-2Mix dataset, we mix various speakers in the `Trainval` subset, ensuring that there is no overlap between the training and validation sets. We follow the same TIR range as in LRS2-2Mix.

2) *Audiovisual Speaker Separation in Noisy Environments:* We use the NTCD-TIMIT dataset [47], recorded in controlled environments, and the LRS3+WHAM! dataset. Both are pre-processed to extract the lip region from the video recordings, following the approach suggested in [18]. The NTCD-TIMIT dataset is designed for noise-robust audiovisual speech recognition for single speakers. To create mixtures of two speakers with noise, we randomly select a second speaker from the same dataset, ensuring that no overlap exists in speakers or utterance contents. TIR is set to 0 dB for speech signals, while the noise signal is uniformly sampled in the signal-to-noise ratio (SNR) range  $[-5, 20]$  dB with mixed signal considered as signal. The dataset has 39 training, 8 validation, and 9 test speakers, with 5 hours of training data, 1 hour of validation data, and 1 hour of test data.

The LRS3+WHAM! dataset combines audiovisual data from LRS3 [45] with noise data from WHAM! [48]. We generate synthetic mixtures of two speakers plus noise. The TIR of clean speech mixtures is uniformly sampled in the range of  $[-5, 5]$  dB, and SNR is in the range of  $[-6, 3]$  dB, following the original mixing process from WHAM!. The LRS3+ WHAM! dataset provides 28 hours of training data, 3 hours of validation data, and 2 hours of test data.

3) *Audiovisual Target Speaker Extraction:* To assess AV-CrossNet’s performance on the AVTSE task, we utilize the VoxCeleb2 [19] dataset for training. This dataset contains over one million utterances from YouTube videos, in a variety of video resolutions and acoustic environments. In order to build the training, validation, and test datasets, we ensure that speakers in the training dataset are not included in the test dataset and all utterances are longer than four seconds. For the training, validation, and test datasets, we generate 20,000, 5,000, and 3,000 mixtures of two speakers, respectively. We introduce a competing speaker to the target speech by randomly sampling a TIR in the range of -10 to 10 dB. In addition to the VoxCeleb2 dataset, we examine AV-CrossNet’s performance on two other untrained datasets, LRS3 [45] and TCD-TIMIT [49]. In each case, we generate 3,000 mixtures similar to [33], [34], [50].

4) *Audiovisual Speech Enhancement:* We use the second COG-MHEAR challenge dataset [39] for AVSE and further AVTSE evaluations. The speech signals in this dataset are collected from the LRS3 dataset [45]. The noise signals are collected from three sources, the domestic noises from the Clarity challenge [51], the Demand noise set [52], and the Freesound noise set from the second DNS challenge [53]. From the COG-MHEAR training set, we select the utterances of 24 speakers with the largest number of utterances to create the validation dataset, resulting in 1339 utterances for AVSE and 1358 utterances for AVTSE. The remaining ones form the training dataset. We treat the development set as the test dataset. The number of training, validation, and test utterances are 30,297, 3,017, and 3,306. The lengths of both the training and validation utterances are 3.0 seconds. Test utterance lengths range from around two seconds to over thirty seconds. This dataset adopts speech-weighted SNRs which are randomly drawn from  $[-10, 10]$  dB and  $[-15, 5]$  dB, for AVSE and AVTSE respectively.

## B. DNN Configuration

For the proposed AV-CrossNet architecture, we make use of the hyperparameters in [40]. We set the kernel size of the audio encoder layer  $k_a$ , time-dimension group convolution (T-GConv1d), and frequency-dimension group convolution (F-GConv1d) to 5, 5, and 3, respectively. The number of groups for T-GConv1d, F-GConv1d, and group normalization is all set to 8. The proposed model comprises  $B = 12$  blocks, with hidden channel sizes set to  $H = 192$ ,  $H' = 16$ , and  $H'' = 384$ . We employ  $N = 4$  self-attention heads in the GMHSA module with an embedding dimension  $E = \lceil 512/F \rceil$ , where  $\lceil \cdot \rceil$  denotes ceiling operation.

To process the input data, we apply STFT using a Hanning window with frame length of 512 samples (32 ms) and frame shift of 256 samples (16 ms). We employ  $R = 5$  V-TCN blocks, where the convolutional layers utilize a stride of 1. The output from the V-TCN blocks is then passed into a Conv1D layer with a kernel size of 3 and 512 output channels.

We utilize the Adam optimization algorithm with a maximum learning rate of  $10^{-3}$ . Initially, we utilize a cosine warm-up scheduler that gradually increases the learning rate from  $10^{-6}$  to  $10^{-3}$  over the first 10 epochs, similar to the approach described in [40]. Subsequently, we transition to the PyTorch ReduceLRonPlateau scheduler, setting the patience to 3 epochs and the reduction factor to 0.9. To reduce memory requirements and accelerate training, we adopt the half-precision (mixed-16) training strategy in our experiments. The model training continues until the validation loss fails to improve for 10 consecutive epochs. For each experiment, we utilize the maximum number of batches that can fit into the GPU memory (NVIDIA A100 GPU with 40 GB of memory).

## C. Evaluation Metrics

To evaluate AV-CrossNet’s performance, we use several common objective metrics. These include: SI-SDR and its improvement, SI-SDRi [54], SDR and its improvement [55], scale-invariant SNR, narrow- and wide-band perceptual evaluation of speech quality (PESQ) [56], and extended short-time objective intelligibility (eSTOI) [57].

To compute these metrics, we employ the TorchMetrics[audio] package [58], which provides a set of evaluation tools designed specifically for audio-related tasks. For calculating narrow-band PESQ, we use the *pypesq* package<sup>1</sup> as done in [36], [46].

## V. EXPERIMENTAL RESULTS AND COMPARISONS

### A. Audiovisual Speaker Separation in Clean Environments

Table I presents AV-CrossNet’s AVSS results in clean environments and compares to those of strong comparison approaches on three LRS2, LRS3, and VoxCeleb2 datasets. Results are reported in terms of SI-SNRi, SDRi, and PESQ. The table also provides the number of trainable parameters and domain of operation for each model.

On LRS2, AV-CrossNet obtains an SI-SNRi of 16.8 dB, outperforming the recently-posted, previous best IANet by

0.8 dB. Its SDRi of 17.1 dB improves upon IANet’s 16.2 dB by 0.9 dB. AV-CrossNet’s PESQ of 3.56 represents a large improvement over IANet’s 3.23. Clear from the table, there is a considerable performance gap between the best AV and audio-only models on all datasets, demonstrating the contribution of the visual stream. On LRS3, AV-CrossNet matches the 18.3 dB SI-SNRi and 18.5 dB SDRi achieved by IANet, but exceeds IANet’s PESQ score by a large margin of 0.39, reaching 3.67 PESQ.

VoxCeleb2 is a more challenging dataset, and AV-CrossNet achieves the state-of-the-art scores of 14.6 dB SI-SNRi, 14.9 dB SDRi, and 3.41 PESQ. These results outperform the previous best-performing model of IANet by 1.0 dB SI-SNRi, 0.6 dB SDRi, and 0.29 PESQ.

As described earlier, AV-CrossNet does not explicitly address the permutation ambiguity issue. Instead we exploit the fact that the visual stream only contains one speaker, and hence it does not pose a permutation issue. In other words, we leverage audiovisual integration to resolve the permutation ambiguity problem. The above compelling separation results demonstrate that permutation ambiguity can be entirely avoided in audiovisual speaker separation.

### B. Audiovisual Speaker Separation in Noisy Environments

Table II reports AV-CrossNet’s AVSS performance in noisy environments and compares to several audio-only and audiovisual methods on two benchmark datasets: NTCD-TIMIT and LRS3+WHAM!. Results are reported in terms of PESQ, eSTOI, and SI-SDRi. On the NTCD-TIMIT dataset, AV-CrossNet achieves the best scores across all three metrics, substantially outperforming current state-of-the-art models. For example, our model obtains the PESQ value of 2.16, a large improvement over the previous best VisualVoice with 1.45 PESQ. For eSTOI, AV-CrossNet obtains 0.62, exceeding AVLiT’s 0.45 by 0.17. AV-CrossNet’s SI-SDRi of 15.6 dB represents a 4.6 dB gain over AVLiT. Compared to the top audio-only models of DPRNN the improvements are even more pronounced.

On the more challenging LRS3+WHAM! dataset, AV-CrossNet maintains the best performance with a PESQ of 2.03, surpassing AVLiT by 0.51. Its eSTOI of 0.77 improves upon AVLiT’s 0.68 by 0.09. For SI-SDRi, AV-CrossNet achieves 13.84 dB, a 1.42 dB increase over AVLiT’s previous best of 12.42 dB. The best audio-only model of DPRNN scores 10.93 dB SI-SDRi. These consistent and often large performance improvements demonstrate AV-CrossNet’s superior ability for speech separation and enhancement across different datasets and metrics.

### C. Audiovisual Target Speaker Extraction

Table III reports AV-CrossNet’s AVTSE performance and those of several recent audiovisual methods on three benchmark datasets: LRS3, TCD-TIMIT, and VoxCeleb2. Results are given in terms of SI-SDR and PESQ. All models in Table III utilize the same visual embedding extractor and are trained only on VoxCeleb2, and tested on LRS3, TCD-TIMIT, and VoxCeleb2 datasets to assess their generalization capabilities.

<sup>1</sup><https://github.com/vBaiCai/python-pesq>

TABLE I: Speaker separation results of different AVSS methods on LRS2, LRS3, and VoxCeleb2 datasets. "Mod." stands for modality, which is either audio-only (A) or audiovisual (AV). The results of comparison methods are adopted from [46] and [36].

Method	Params (M)	Domain	Mod.	LRS2			LRS3			VoxCeleb2		
				SI-SNRi	SDRi	PESQ	SI-SNRi	SDRi	PESQ	SI-SNRi	SDRi	PESQ
Unprocessed				0.0	0.0	1.71	0.0	0.0	1.73	0.0	0.0	1.89
DPCL++ [4]	13.6	T-F	A	3.3	4.3	–	5.8	6.2	–	2.1	2.5	–
Conv-TasNet [6]	5.6	Time	A	10.3	10.7	–	11.1	11.4	–	6.9	7.5	–
SuDoRM-RF [59]	2.7	Time	A	9.1	9.5	–	12.1	12.3	–	6.5	6.9	–
A-FRCNN [60]	6.3	Time	A	9.4	10.1	–	12.5	12.8	–	7.8	8.2	–
The Conversation [27]	62.7	T-F	AV	–	–	–	–	–	–	–	8.9	–
AVConvTasNet [33]	16.45	Time	AV	12.5	12.8	2.69	11.2	11.7	2.58	9.2	9.8	2.17
LWTNet [61]	69.4	T-F	AV	–	10.8	–	–	4.8	–	–	–	–
Visualvoice [32]	77.8	T-F	AV	11.5	11.8	2.78	9.9	10.3	2.13	9.3	10.2	2.45
CaffNet-C [62]		T-F	AV	–	10.0	–	–	9.8	–	–	7.6	–
CTCNet [46]	7.0	Time	AV	14.3	14.6	3.08	17.4	17.5	3.24	11.9	13.1	3.00
AVLiT [63]	5.75	Time	AV	12.8	13.1	2.56	13.5	13.6	2.78	9.4	9.9	2.23
IIANet [36]	3.1	Time	AV	16.0	16.2	3.23	<b>18.3</b>	<b>18.5</b>	3.28	13.6	14.3	3.12
AVSepChain [64]	33.1	Time	AV	15.3	15.7	3.26	–	–	–	13.6	14.2	2.72
<b>AV-CrossNet</b>	11.1	T-F	AV	<b>16.8</b>	<b>17.1</b>	<b>3.56</b>	<b>18.3</b>	<b>18.5</b>	<b>3.67</b>	<b>14.6</b>	<b>14.9</b>	<b>3.41</b>

TABLE II: Speaker separation results of AV-CrossNet and baseline models on NTCD-TIMIT and LRS3+WHAM! datasets. Comparison results are from [63].

Method	Mod.	NTCD-TIMIT			LRS3+WHAM!		
		PESQ	eSTOI	SI-SDRi	PESQ	eSTOI	SI-SDRi
Unprocessed		1.19	0.33	–	1.08	0.37	–
ConvTasNet [6]	A	1.35	0.38	8.76	1.24	0.51	9.66
DPRNN [65]	A	1.32	0.39	9.31	1.40	0.45	10.93
A-FRCNN [60]	A	1.30	0.31	6.92	1.25	0.49	9.21
AVConvTasNet [33]	AV	1.33	0.40	9.02	1.29	0.60	6.21
LAVSE [66]	AV	1.31	0.37	6.22	1.24	0.50	5.59
L2L [20]	AV	1.23	0.26	3.36	1.16	0.51	7.60
VisualVoice [32]	AV	1.45	0.43	10.04	1.48	0.63	11.87
AVLiT [63]	AV	1.43	0.45	11.00	1.52	0.68	12.42
<b>AV-CrossNet</b>	AV	<b>2.16</b>	<b>0.62</b>	<b>15.6</b>	<b>2.03</b>	<b>0.77</b>	<b>13.84</b>

On the LRS3 dataset, AV-CrossNet achieves the state-of-the-art SI-SDR of 17.42 dB, outperforming the recently posted previous best AV-SepChain by 2.22 dB. Its PESQ of 3.14 represents a marginal improvement of 0.02 over AV-SepChain. Similarly, on TCD-TIMIT, AV-CrossNet achieves the best results with 18.15 dB SI-SDR and 3.25 PESQ, showing an improvement of 3.45 dB SI-SDR and 0.37 in PESQ over AV-SepChain. On the VoxCeleb2 dataset used for training, AV-CrossNet again outperforms all previous methods, achieving 14.71 dB SI-SDR and 2.93 PESQ. The improvements over AV-SepChain are 0.51 dB in SI-SDR and 0.21 in PESQ, highlighting the consistently high performance of AV-CrossNet in leveraging audiovisual cues for improved speech separation. Overall, these results establish AV-CrossNet as the new leading method for audiovisual target speaker extraction across diverse audiovisual datasets.

In Fig. 3, we break down our SI-SDR results on three datasets in different ranges of unprocessed SNR (dB). As il-

lustrated in this figure, AV-CrossNet produces excellent results over all input SNR range. It is worth noting that, as the input SNR range varies over 17 dB – from [-10, -7] to (7, 10] – the processed SI-SDR results vary within a considerably smaller range, about half of 17 dB. This shows that AV-CrossNet yields relatively better performance at lower SNRs, likely due to the more prominent role of the visual modality with decreasing SNR.

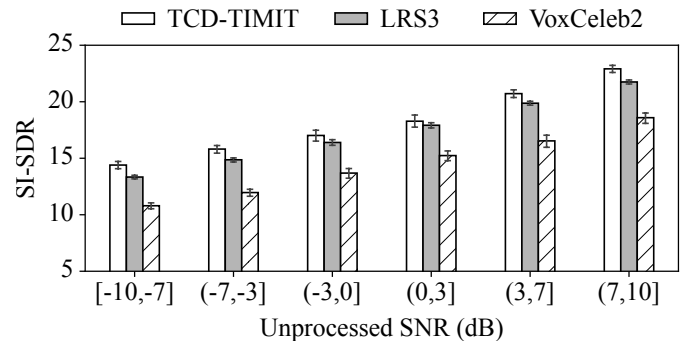


Fig. 3: SI-SDR results of AV-CrossNet across different SNRs for unprocessed mixtures on the test datasets TCD-TIMIT, LRS3, and VoxCeleb2. Error bars represent 95% confidence intervals.

To gain further insight into AV-CrossNet’s target speaker extraction performance, we analyze test results on the untrained TCD-TIMIT dataset [49]. Fig. 4 breaks down results in various gender pairs. A pair is denoted in the order of target and interferer; for example, MF denotes a male target speaker mixed with a female interfering speaker. We select SI-SDR and PESQ metrics to present our analysis. We observe that AV-CrossNet performs better in mixed-gender pairs, not surprisingly. FM pairs are easier to extract than MF pairs. This could be attributed to the higher fundamental frequencies

TABLE III: Target speaker extraction results of AV-CrossNet and baseline models on LRS3, TCD-TIMIT, and VoxCeleb2. All models use the same visual embedding extractor and are trained on the VoxCeleb2 dataset.

Method	LRS3		TCD-TIMIT		VoxCeleb2	
	SI-SDR	PESQ	SI-SDR	PESQ	SI-SDR	PESQ
Unprocessed	0.13	1.21	-0.15	1.47	-0.08	1.24
VisualVoice [32]	11.60	2.27	10.88	2.25	9.73	1.97
AV-ConvTasNet [33]	12.13	2.33	11.53	2.21	10.38	1.97
MuSE [34]	12.97	2.56	12.50	2.45	11.24	2.20
AV-SepFormer [50]	13.81	2.67	13.44	2.57	12.13	2.31
AVSepChain [64]	15.2	3.12	14.7	2.88	14.2	2.72
<b>AV-CrossNet</b>	<b>17.42</b>	<b>3.14</b>	<b>18.15</b>	<b>3.25</b>	<b>14.71</b>	<b>2.93</b>

of female speakers, which lead to neighboring harmonics more separated in frequency, facilitating their extraction. In same-gender scenarios, FF pairs yield better results than MM pairs. These findings are generally consistent with the previous findings such as those in [20].

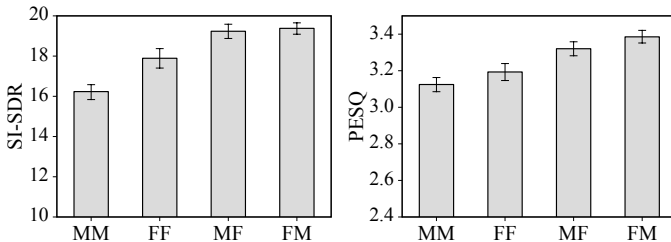


Fig. 4: Target speaker extraction results of different gender pairs. The first and second letters denote the genders of the target and interfering speakers, respectively.

#### D. COG-MHEAR AVSE Challenge

Table IV presents AV-CrossNet’s result and compares to the previous state-of-the-art methods on the COG-MHEAR challenge. AV-DPRNN [38] is a time-domain audiovisual model that performs end-to-end audiovisual processing, and is jointly trained on both AVSE and AVTSE for this challenge. AV-GridNet also performs complex spectral mapping, and its results are reported in several training setups. AV-GridNet<sub>all</sub> is trained in both AVSE and AVTSE scenarios. AV-GridNet<sub>s</sub> and AV-GridNet<sub>n</sub> are expert models trained separately for AVTSE and AVSE, respectively. SAV-GridNet denotes the best-performing system on COG-MHEAR challenge that includes two expert models and a scenario classifier. This model has around 22M parameters, aiming to process noisy speech in matched scenarios. As shown in Table IV, AV-CrossNet with around 11M parameters outperforms AV-GridNet<sub>all</sub> by 0.13 PESQ and at least 0.4 dB SI-SDR on both AVSE and AVTSE tasks. Notably, AV-CrossNet also outperforms the more sophisticated two-stage system of SAV-GridNet by a substantial margin on AVSE; AV-CrossNet and SAV-GridNet achieve comparable results on the AVTSE task. We note that, although the scenario classifier achieves the classification accuracy of 99.4% on this particular task, distinguishing speech

enhancement and target speaker extraction is likely error-prone in realistic environments that contain both overlapped speech and background noise. The performance gap between AV-GridNet<sub>all</sub> and AV-CrossNet shows the latter’s versatility in both scenarios.

TABLE IV: Evaluation results of AV-CrossNet and baseline models on the development set for the second COG-MHEAR Audiovisual Speech Enhancement Challenge.

Method	Speech+Noise			Speech+Speech		
	PESQ	STOI	SI-SDR	PESQ	STOI	SI-SDR
Unprocessed	1.15	0.68	-4.4	1.17	0.60	-5.0
AV-DPRNN [38]	2.02	0.86	11.4	2.23	0.90	12.6
AV-GridNet <sub>all</sub> [38]	2.62	0.91	13.9	3.10	<b>0.95</b>	16.7
AV-GridNet <sub>s</sub> [38]	2.56	0.90	13.4	<b>3.23</b>	<b>0.95</b>	<b>17.5</b>
AV-GridNet <sub>n</sub> [38]	2.68	0.91	14.2	1.27	0.61	-4.7
SAV-GridNet [38]	2.68	0.91	14.2	<b>3.23</b>	<b>0.95</b>	<b>17.5</b>
<b>AV-CrossNet</b>	<b>2.75</b>	<b>0.92</b>	<b>14.3</b>	<b>3.23</b>	<b>0.95</b>	17.3

## VI. CONCLUSION

We have presented AV-CrossNet for single-channel audiovisual speech enhancement, audiovisual speaker separation, and audiovisual target speaker extraction tasks. This system is based on the CrossNet architecture and integrates a visual front-end using the DeepAVSR model to extract embeddings from video frames. AV-CrossNet comprises an audio encoder, a visual encoder, separator blocks, and a decoder. The proposed model leverages narrow- and cross-band modeling as well as global attention to estimate the real and imaginary spectrogram of an individual speaker. By virtue of audiovisual processing, AV-CrossNet is not susceptible to the permutation ambiguity problem in talker-independent speaker separation. The proposed model achieves superior performance across a number of audiovisual datasets, even on untrained challenging datasets, and establishes new state-of-the-art results on these datasets.

## VII. ACKNOWLEDGEMENTS

This work was supported in part by a Meta contract to Ohio State University, the Ohio Supercomputer Center, the NCSA Delta Supercomputer Center (OCI 2005572), and the Pittsburgh Supercomputer Center (NSF ACI-1928147).

## REFERENCES

- [1] D. L. Wang and J. Chen, “Supervised speech separation based on deep learning: An overview,” *IEEE Trans. Audio, Speech, Lang. Process.*, vol. 26, pp. 1702–1726, 2018.
- [2] P. C. Loizou, *Speech Enhancement: Theory and Practice*. CRC press, 2013.
- [3] D. L. Wang and G. J. Brown, *Computational auditory scene analysis: Principles, algorithms, and applications*. Wiley-IEEE press, 2006.
- [4] J. R. Hershey, Z. Chen, J. Le Roux, and S. Watanabe, “Deep Clustering: Discriminative embeddings for segmentation and separation,” in *Proc. ICASSP*, 2016, pp. 31–35.
- [5] M. Kolbæk, D. Yu, Z.-H. Tan, and J. Jensen, “Multitalker speech separation with utterance-level permutation invariant training of deep recurrent neural networks,” *IEEE Trans. Audio, Speech, Lang. Proc.*, vol. 25, pp. 1901–1913, 2017.



- [6] Y. Luo and N. Mesgarani, "Conv-TasNet: Surpassing ideal time-frequency magnitude masking for speech separation," *IEEE Trans. Audio, Speech, Lang. Process.*, vol. 27, pp. 1256–1266, 2019.
- [7] Y. Liu and D. L. Wang, "Divide and Conquer: A deep CASA approach to talker-independent monaural speaker separation," *IEEE Trans. Audio, Speech, Lang. Process.*, vol. 27, pp. 2092–2102, 2019.
- [8] Y. Luo, Z. Chen, and T. Yoshioka, "Dual-path RNN: Efficient long sequence modeling for time-domain single-channel speech separation," in *Proc. ICASSP*, 2020, pp. 46–50.
- [9] Z.-Q. Wang, S. Cornell, S. Choi, Y. Lee, B.-Y. Kim, and S. Watanabe, "TF-GridNet: Integrating full-and sub-band modeling for speech separation," *IEEE Trans. Audio, Speech, Lang. Process.*, vol. 31, pp. 3221–3236, 2023.
- [10] S. Dovrat, E. Nachmani, and L. Wolf, "Many-speakers single channel speech separation with optimal permutation training," *arXiv:2104.08955*, 2021.
- [11] T. von Neumann, K. Kinoshita, C. Boeddeker, M. Delcroix, and R. Haeb-Umbach, "Segment-less continuous speech separation of meetings: Training and evaluation criteria," *IEEE Trans. Audio, Speech, Lang. Process.*, vol. 31, pp. 576–589, 2022.
- [12] H. Taherian and D. L. Wang, "Multi-channel conversational speaker separation via neural diarization," *IEEE Trans. Audio, Speech, Lang. Process.*, vol. 32, pp. 2467–2476, 2024.
- [13] Q. Wang, H. Muckenhirn, K. Wilson, P. Sridhar, Z. Wu, J. Hershey, R. A. Saurous, R. J. Weiss, Y. Jia, and I. L. Moreno, "VoiceFilter: Targeted voice separation by speaker-conditioned spectrogram masking," *arXiv:1810.04826*, 2018.
- [14] A. Pandey and D. L. Wang, "Attentive training: A new training framework for speech enhancement," *IEEE Trans. Audio, Speech, Lang. Process.*, vol. 31, pp. 1360–1370, 2023.
- [15] D. Michelsanti, Z.-H. Tan, S.-X. Zhang, Y. Xu, M. Yu, D. Yu, and J. Jensen, "An overview of deep-learning-based audio-visual speech enhancement and separation," *IEEE Trans. Audio, Speech, Lang. Process.*, vol. 29, pp. 1368–1396, 2021.
- [16] W. H. Sumby and I. Pollack, "Visual contribution to speech intelligibility in noise," *The Journal of the Acoustical Society of America*, vol. 26, pp. 212–215, 1954.
- [17] M. J. Crosse, G. M. Di Liberto, and E. C. Lalor, "Eye can hear clearly now: inverse effectiveness in natural audiovisual speech processing relies on long-term crossmodal temporal integration," *Journal of Neuroscience*, vol. 36, pp. 9888–9895, 2016.
- [18] T. Afouras, J. S. Chung, A. Senior, O. Vinyals, and A. Zisserman, "Deep audio-visual speech recognition," *IEEE Tans. Pattern Analysis and Machine Intelligence*, vol. 44, pp. 8717–8727, 2018.
- [19] J. S. Chung, A. Nagrani, and A. Zisserman, "VoxCeleb2: Deep speaker recognition," *arXiv:1806.05622*, 2018.
- [20] A. Ephrat, I. Mosseri, O. Lang, T. Dekel, K. Wilson, A. Hassidim, W. T. Freeman, and M. Rubinstein, "Looking to listen at the cocktail party: a speaker-independent audio-visual model for speech separation," *arXiv:1804.03619*, 2018.
- [21] K. Tan, Y. Xu, S.-X. Zhang, M. Yu, and D. Yu, "Audio-visual speech separation and dereverberation with a two-stage multimodal network," *IEEE Journal of Selected Topics in Signal Processing*, vol. 14, pp. 542–553, 2020.
- [22] S. Tamura, H. Ninomiya, N. Kitaoka, S. Osuga, Y. Iribe, K. Takeda, and S. Hayamizu, "Audio-visual speech recognition using deep bottleneck features and high-performance lipreading," in *Asia-Pacific Signal and Information Processing Association Conference*, 2015, pp. 575–582.
- [23] P. Ma, A. Haliassos, A. Fernandez-Lopez, H. Chen, S. Petridis, and M. Pantic, "Auto-AVSR: Audio-visual speech recognition with automatic labels," in *Proc. ICASSP*, 2023, pp. 1–5.
- [24] M. Sadeghi and X. Alameda-Pineda, "Mixture of inference networks for VAE-based audio-visual speech enhancement," *arXiv:1912.10647*, 2019.
- [25] Y. Li, Z. Liu, Y. Na, Z. Wang, B. Tian, and Q. Fu, "A visual-pilot deep fusion for target speech separation in multitalker noisy environment," in *Proc. ICASSP*, 2020, pp. 4442–4446.
- [26] T. Ochiai, M. Delcroix, K. Kinoshita, A. Ogawa, and T. Nakatani, "Multimodal SpeakerBeam: Single channel target speech extraction with audio-visual speaker clues," in *Proc. Interspeech*, 2019, pp. 2718–2722.
- [27] T. Afouras, J. S. Chung, and A. Zisserman, "The conversation: deep audio-visual speech enhancement," *arXiv:1804.04121*, 2018.
- [28] —, "My lips are concealed: Audio-visual speech enhancement through obstructions," *arXiv:1907.04975*, 2019.
- [29] S.-W. Chung, S. Choe, J. S. Chung, and H.-G. Kang, "FaceFilter: Audio-visual speech separation using still images," in *Proc. Interspeech*, 2020, pp. 3481–3485.
- [30] A. Gabbay, A. Shamir, and S. Peleg, "Visual speech enhancement," in *Proc. Interspeech*, 2018, pp. 1170–1174.
- [31] A. Gabbay, A. Ephrat, T. Halperin, and S. Peleg, "Seeing through noise: Visually driven speaker separation and enhancement," in *Proc. ICASSP*, 2018, pp. 3051–3055.
- [32] R. Gao and K. Grauman, "VisualVoice: Audio-visual speech separation with cross-modal consistency," in *Proc. CVPR*, 2021, pp. 15 490–15 500.
- [33] J. Wu, Y. Xu, S.-X. Zhang, L.-W. Chen, M. Yu, L. Xie, and D. Yu, "Time domain audio visual speech separation," in *Proc. IEEE ASRU*, 2019, pp. 667–673.
- [34] Z. Pan, R. Tao, C. Xu, and H. Li, "MuSE: Multi-modal target speaker extraction with visual cues," in *Proc. ICASSP*, 2021, pp. 6678–6682.
- [35] V. A. Kalkhorani, A. Kumar, K. Tan, B. Xu, and D. L. Wang, "Time-domain transformer-based audiovisual speaker separation," in *Proc. Interspeech*, 2023, pp. 3472–3476.
- [36] K. Li, R. Yang, F. Sun, and X. Hu, "IINet: An intra- and inter-modality attention network for audio-visual speech separation," *arXiv:2308.08143*, 2024.
- [37] V. A. Kalkhorani, A. Kumar, K. Tan, B. Xu, and D. L. Wang, "Audio-visual speaker separation with full-and sub-band modeling in the time-frequency domain," in *Proc. ICASSP*, 2024, pp. 12 001–12 005.
- [38] Z. Pan, G. Wichern, Y. Masuyama, F. G. Germain, S. Khurana, C. Hori, and J. L. Roux, "Scenario-aware audio-visual TF-GridNet for target speech extraction," *arXiv:2310.19644*, 2023.
- [39] A. L. A. Blanco, C. Valentini-Botinhao, O. Klejch, M. Gogate, K. Dashtipour, A. Hussain, and P. Bell, "AVSE Challenge: audio-visual speech enhancement challenge," in *Proc. IEEE Spok. Lang. Tech. Work.*, 2023, pp. 465–471.
- [40] V. A. Kalkhorani and D. L. Wang, "CrossNet: Leveraging global, cross-band, narrow-band, and positional encoding for single- and multi-channel speaker separation," *arXiv: 2403.03411*, 2024.
- [41] C. Lea, R. Vidal, A. Reiter, and G. D. Hager, "Temporal Convolutional Networks: A unified approach to action segmentation," in *Proc. ECCV*, 2016, pp. 47–54.
- [42] A. Vaswani, N. Shazeer, N. Parmar, J. Uszkoreit, L. Jones, A. N. Gomez, L. Kaiser, and I. Polosukhin, "Attention is all you need," *Adv. Neural Info. Proc. Sys.*, vol. 30, 2017.
- [43] C. Quan and X. Li, "SpatialNet: Extensively learning spatial information for multichannel joint speech separation, denoising and dereverberation," *IEEE Trans. Audio, Speech, Lang. Process.*, vol. 32, pp. 1310–1323, 2024.
- [44] Z. Pan, M. Ge, and H. Li, "A hybrid continuity loss to reduce over-suppression for time-domain target speaker extraction," *arXiv:2203.16843*, 2022.
- [45] T. Afouras, J. S. Chung, and A. Zisserman, "LRS3-TED: A large-scale dataset for visual speech recognition," *arXiv:1809.00496*, 2018.
- [46] K. Li, F. Xie, H. Chen, K. Yuan, and X. Hu, "An audio-visual speech separation model inspired by cortico-thalamo-cortical circuits," *arXiv:2212.10744*, 2022.
- [47] A. H. Abdelaziz *et al.*, "NTCD-TIMIT: A new database and baseline for noise-robust audio-visual speech recognition," in *Proc. Interspeech*, 2017, pp. 3752–3756.
- [48] G. Wichern, J. Antognini, M. Flynn, L. R. Zhu, E. McQuinn, D. Crow, E. Manilow, and J. L. Roux, "WHAM!: Extending speech separation to noisy environments," *arXiv:1907.01160*, 2019.
- [49] N. Harte and E. Gillen, "TCD-TIMIT: An audio-visual corpus of continuous speech," *IEEE Trans. Multimedia*, vol. 17, pp. 603–615, 2015.
- [50] J. Lin, X. Cai, H. Dinkel, J. Chen, Z. Yan, Y. Wang, J. Zhang, Z. Wu, Y. Wang, and H. Meng, "AV-Sepformer: Cross-attention sepformer for audio-visual target speaker extraction," in *Proc. ICASSP*, 2023, pp. 1–5.
- [51] S. Graetzer, J. Barker, T. J. Cox, M. Akeroyd, J. F. Culling, G. Naylor, E. Porter, and R. Viveros Munoz, "Clarity-2021 challenges: Machine learning challenges for advancing hearing aid processing," in *Proc. Interspeech*, 2021, pp. 686–690.
- [52] J. Thiemann, N. Ito, and E. Vincent, "DEMAND: A collection of multi-channel recordings of acoustic noise in diverse environments," in *Meetings Acoust.*, 2013, pp. 1–6.
- [53] H. Dubej, A. Aazami, V. Gopal, B. Naderi, S. Braun, R. Cutler, A. Ju, M. Zohourian, M. Tang, M. Golestaneh, and R. Aichner, "Proc. ICASSP 2023 deep noise suppression challenge," in *Proc. ICASSP*, 2023, pp. 1–13.
- [54] J. Le Roux, S. Wisdom, H. Erdogan, and J. R. Hershey, "SDR-half-baked or well done?" in *Proc. ICASSP*, 2019, pp. 626–630.
- [55] E. Vincent, R. Gribonval, and C. Févotte, "Performance measurement in blind audio source separation," *IEEE Trans. Audio, Speech, Lang. Process.*, vol. 14, pp. 1462–1469, 2006.

- [56] A. W. Rix, J. G. Beerends, M. P. Hollier, and A. P. Hekstra, "Perceptual evaluation of speech quality (PESQ)-a new method for speech quality assessment of telephone networks and codecs," in *Proc. ICASSP*, 2001, pp. 749–752.
- [57] J. Jensen and C. H. Taal, "An algorithm for predicting the intelligibility of speech masked by modulated noise maskers," *IEEE Tran. Audio, Speech, Lang. Process.*, vol. 24, pp. 2009–2022, 2016.
- [58] N. S. Detlefsen, J. Borovec, J. Schock, A. H. Jha, T. Koker, L. Di Liello, D. Stancil, C. Quan, M. Grechkin, and W. Falcon, "TorchMetrics-measuring reproducibility in pytorch," *Journal of Open Source Software*, vol. 7, p. 4101, 2022.
- [59] E. Tzinis, Z. Wang, and P. Smaragdis, "SuDoRM-RF: Efficient networks for universal audio source separation," in *Proc. MLSP*, 2020, pp. 1–6.
- [60] X. Hu, K. Li, W. Zhang, Y. Luo, J.-M. Lemercier, and T. Gerkmann, "Speech separation using an asynchronous fully recurrent convolutional neural network," in *Proc. NeurIPS*, vol. 34, 2021, pp. 22 509–22 522.
- [61] T. Afouras, A. Owens, J. S. Chung, and A. Zisserman, "Self-supervised learning of audio-visual objects from video," in *Proc. Computer Vision–ECCV*, 2020, pp. 208–224.
- [62] J. Lee, S.-W. Chung, S. Kim, H.-G. Kang, and K. Sohn, "Looking into your speech: learning cross-modal affinity for audio-visual speech separation," in *Proc. CVPR*, 2021, pp. 1336–1345.
- [63] H. Martel, J. Richter, K. Li, X. Hu, and T. Gerkmann, "Audio-visual speech separation in noisy environments with a lightweight iterative model," *arXiv:2306.00160*, 2023.
- [64] Z. Mu and X. Yang, "Separate in the Speech Chain: Cross-modal conditional audio-visual target speech extraction," *arXiv:2404.12725*, 2024.
- [65] Y. Luo, Z. Chen, and T. Yoshioka, "Dual-Path RNN: Efficient long sequence modeling for time-domain single-channel speech separation," in *Proc. ICASSP*, 2020, pp. 46–50.
- [66] S.-Y. Chuang, Y. Tsao, C.-C. Lo, and H.-M. Wang, "Lite audio-visual speech enhancement," *arXiv:2005.11769*, 2020.